From isochorismate to salicylate: a new reaction mechanism for salicylic acid biosynthesis

Dmitrij Rekhter[1], Yuli Ding[2], Daniel Lüdke[3], Kirstin Feussner[1,4], Marcel Wiermer[3], Yuelin Zhang[2,*], Ivo Feussner[1,5,*]

[1] University of Goettingen, Albrecht-von-Haller-Institute for Plant Sciences, Department of Plant Biochemistry, D-37077 Goettingen, Germany.

[2] University of British Columbia, Department of Botany, Vancouver, BC V6T 1Z4, Canada.

[3] University of Goettingen, Albrecht-von-Haller-Institute for Plant Sciences, RG Molecular Biology of Plant-Microbe Interactions, D-3707 Goettingen, Germany.

[4] University of Goettingen, Goettingen Center for Molecular Biosciences (GZMB), Service Unit for Metabolomics and Lipidomics, D-37077 Goettingen, Germany.

[5] University of Goettingen, Goettingen Center for Molecular Biosciences (GZMB), Department of Plant Biochemistry, D-37077 Goettingen, Germany.

*Correspondence to Ivo Feussner: ifeussn@uni-goettingen.de or Yuelin Zhang: yuelin.zhang@ubc.ca.

Abstract: Salicylic acid (SA) is an essential regulator of plant immune responses. Despite decades of research, our knowledge of its biosynthesis remains incomplete. Here we report that by conjugating glutamate to isochorismic acid, avrPphB Susceptible 3 (PBS3) catalyzes the formation of Isochorismate-9-glutamate (ISC-9-Glu), which then further decays into SA without the requirement of any enzymatic catalysis. Thus, plant SA biosynthesis can be reconstituted with just the two enzymes Isochorismate Synthase 1 (ICS1) and PBS3, along with the putative isochorismate transporter Enhanced Disease Susceptibility 5 (EDS5). This is the very first example of a decay-driven biosynthesis of a phytohormone.

One Sentence Summary: PBS3 produces SA via Isochorismate-9-glutamate.

Main Text: Salicylic acid (SA) is a plant defense hormone with central functions in regulating plant immune responses (*1*). The crucial role of SA as the modulator of local as well as systemic immune response has been studied extensively (*2*). Early [^{14}C]-feeding experiments suggested that SA is synthesized from phenylalanine via cinnamic acid (*3, 4*), however, the discovery of Isochorismate Synthase 1 (ICS1) in *Arabidopsis thaliana* showed that ~90% of the pathogen-induced SA is produced via isochorismic acid (ISC) (*5, 6*). SA was proposed to be synthesized in plastids and exported to the cytosol by Enhanced Disease Susceptibility 5 (EDS5), which is a member of the MATE (multidrug and toxin extrusion) transporter family (*7*). This ICS-dependent pathway is known from bacteria, where chorismic acid (CA) is converted to SA either by a bifunctional SA synthase (SAS) or by two separate enzymes, whereby CA is isomerized to ISC first, followed by cleavage through an isochorismate pyruvate lyase (IPL). However, since *Arabidopsis* ICS1 was reported to be a monofunctional enzyme and no IPL could be found in plant genomes (*8*), it remained unclear how ISC is converted to SA in higher plants.

The accumulation of SA and SA-glycoside (SAG) upon *Pseudomonas syringe* infection is reduced, but not abolished in *Arabidopsis pbs3* mutant plants (*9*). *PBS3* encodes an amido transferase of the GH3 family. The founding member of this protein family, AtGH3.11 (JAR1), catalyzes the conjugation of isoleucine to jasmonic acid (JA) to form the hormone conjugate JA-isoleucine (JA-Ile), which represents the active form of JA for signaling (*10*). However, SA was shown to be a poor substrate for PBS3 and even an inhibitor at higher concentrations (*11*) and the function of PBS3 remains to be determined.

To better understand the role of PBS3 in plant defense, we crossed *pbs3-1* into the autoimmune mutant *snc2-1D npr1-1* (suppressor of npr1-1, constitutive 2) which has constitutively activated defense responses (*12*), and performed metabolite fingerprinting analysis. The previously reported *snc2-1D npr1-1 eds5-3* triple mutant (*12*) was used as a control. Similar to *eds5-3*, *pbs3-1* cannot suppress the dwarf phenotype of *snc2-1D npr1-1* (Fig. 1A).

In *snc2-1D npr1-1*, SA (Fig. 1B), SAG (Fig. 1C) and the SA catabolites 2,3- as well as 2,5-dihydroxybenzoic acid xyloside (Fig. 1D and S1) accumulate drastically (*13*). The loss-of-function mutations of either *PBS3* or *EDS5* both lead to dramatically reduced accumulation of SA and its derivatives. Interestingly, we could detect a significant accumulation of the SA precursor ISC in the *snc2-1D npr1-1 pbs3-1* but not in the *snc2-1D npr1-1 eds5-3* mutant (Fig. 1E). Based on these findings, we hypothesized that ISC may be the *in planta* substrate for PBS3.

To verify our hypothesis, we tested whether heterologously expressed and purified PBS3 (Fig. S2) is able to utilize CA for the conjugation with glutamic acid (Glu) (*11*) by monitoring the production of CA-Glu in a mass-spectrometry-based activity assay. Interestingly, the reaction yielded two signals for the enzymatic product CA-Glu (*m/z* 354.083, Fig. 2A red graph). The MS/MS fragmentation analysis showed that both the C7 and the C9 carboxyl group are targets for the amido transferase (CA-7-Glu, CA-9-Glu, Fig.2B a, d, Fig. S3). Next, we examined whether PBS3 also accepts ISC as substrate. As ISC is commercially not available, we used purified recombinant ICS1 to produce ISC from CA (Fig. S4 and S5) and subsequently removed the protein from the reaction by ultrafiltration. Along with residual amounts of CA, ISC was then tested as substrate for PBS3. The PBS3 activity assay yielded four signals of *m/z* 354.083, of which two represent the CA-conjugates (Fig. 2A a and d). The most intense signal (at 2.85 min) was unequivocally identified via MS/MS fragmentation as ISC-9-Glu (Fig. 2A c, 2B c, S3). The structures for the four signals are depicted in Fig. 2B. Assuming that these four compounds have similar ionization properties, we conclude that the formation of ISC-9-Glu (Fig. 2B c) is the preferred reaction of PBS3.

Remarkably, we could also detect the presence of SA in the PBS3 activity assay (Fig. 2C). It is known that ISC itself decays slowly to SA in solution (*14*). Therefore, we investigated if the formation of SA relies on the completeness of the activity assay by omitting individual components of the PBS3 reaction. Indeed, we could detect a small amount of SA in the absence of either Glu, ATP or PBS3 in the enzymatic assay. However, within the first hour of the reaction, the SA signal was four times higher in the presence of Glu, ATP and PBS3 than in the controls. As no lyase activity has been reported for GH3 proteins so far, the formation of ISC-9-Glu most likely strongly enhances the decay of the ISC-backbone, leading to the accumulation of SA.

The activity of GH3 enzymes consists of a two-step reaction. In the first step, an acyl substrate is adenylated under the formation of pyrophosphate, followed by the conjugation of an amino acid

to the activated acyl substrate. Finally, the resulting conjugate as well as adenosine monophosphate (AMP) are released. The kinetic parameters for the PBS3 catalyzed conjugation of Glu with ICS were determined by a spectrophotometric assay (Fig. 2D) (*15*), using the previously investigated acyl substrate 4-hydroxybenzoic acid (4HBA) as a control (*11*). Strikingly, we had to dilute the enzyme one hundred fold when we assessed ISC instead of 4HBA as acyl substrate, as the reaction was otherwise too fast for an accurate measurement. The catalytic efficiency (k_{cat}/K_m) of PBS3 was increased by a factor of ~740 when ISC (31.70 min^{-1} μM^{-1}) was used as the acyl substrate in place of 4HBA (0.043 min^{-1} μM^{-1}), which can be attributed to a much higher substrate affinity (~21-fold) and an enhanced turnover rate (~35-fold) for ISC. These data suggest that ISC is the preferred substrate of PBS3 here. Next, we utilized the publically available crystal structure of PBS3, which was co-crystallized with SA and AMP (PDB ID 4eql) (*16*), to model the possible orientation of ISC within the active center (Fig. S6A). When we superimposed the ring-structure of SA with that of ISC (Fig. S6 B-D), we observed that there is i) sufficient space to accommodate the bulky side chain of the ISC-molecule in the active center and that ii) the phosphate group of the AMP-moiety - and the C9-carboxyl group of ISC are in close proximity (~2.5 Å; Fig. S6C). Based on the high efficiency of PBS3 in catalyzing the conjugation of ISC to Glu and the geometry of the active site, we propose that PBS3 is directly involved in the biosynthesis of SA (Fig. 2E).

Beside SA, we detected 2-hydroxy acryloyl-N-glutamic acid (2HNG, *m/z* 216.051) as the second product of the decay of ISC-9-Glu in the PBS3 *in vitro* assay. To determine whether the decay of ISC-9-Glu also occurs *in vivo*, we analyzed the accumulation of ISC-9-Glu and 2NHG *in planta*. Both compounds were present in *snc2-1D npr1-1* samples, with retention times and mass per charge ratios corresponding to those observed in the *in vitro* enzymatic assay. However, they were neither discovered in *snc2-1D npr1-1 pbs3-1* nor in *snc2-1D npr1-1 eds5-3* triple mutant plants (Fig. 3A and B), which correlates with the accumulation of SA shown in Fig. 1A. We performed MS/MS fragmentation for ISC-9-Glu produced *in vivo* (Fig. 3C) or *in vitro* (Fig. 3D), respectively. The fragmentation patterns were almost identical and all recorded fragments could be assigned unequivocally by their exact mass information (Fig. 3E and F). Based on these data, we conclude that ISC-9-Glu is indeed the direct precursor of SA *in planta*, into which it decays rapidly (Fig. 2E).

We further monitored the non-enzymatic formation of SA originating from the decay of ISC-9-Glu and ISC for 24 h. Within the first 6 h after starting the reaction, ISC-9-Glu shows a linear dissociation rate, which is 10-times higher compared to the corresponding rate observed for ISC (Fig. 3G). After ~20 h, ISC-9-Glu reaches its dissociation equilibrium. At this point, the dissociation of ISC is still in a linear range. In order to understand the accelerated decay, we employed molecular modeling for ISC-9-Glu. The resulting structure (Fig. S7A) strongly suggests the formation of three hydrogen bonds: between the i) alpha and omega carboxyl group of the glutamyl moiety, the ii) carboxyl - respectively hydroxyl group of the ISC ring system, as well as between the iii) amide hydrogen of the peptide bond and the oxygen of the ether bridge. The latter hydrogen bond brings these two functional groups in close proximity and this distance is most likely sufficient to facilitate a hydrogen transfer. As a consequence of this protonation, we expect a base-initiated aromatization of the ring system, which leads to an elimination reaction of the E1 type yielding SA and 2HNG as final products (Fig. S7B). The chemical formation of SA via the non-enzymatic decay may partially explain the delayed accumulation of SA (12 hpi) relative to the induction of the expression of *ICS1*, *PBS3* and *EDS5* (6 hpi) upon pathogen challenge (*17, 18*).

The biosynthesis of SA was proposed to occur in the plastid, as ICS1 was shown to localize to this subcellular compartment (*6*). Interestingly, sequence analyses with the *in silico* online tools TargetP (*19*) and Predotar (*20*) predicted PBS3 to be localized to the cytosol, which is consistent with studies of other GH3 enzymes (*21, 22*). We used *Agrobacterium*-mediated transient expression of PBS3-YFP in *Nicotiana benthamiana* as well as in *Arabidopsis efr* mutant leaves which allow enhanced *Agrobacterium*-mediated transient transformation rates (*23*), but could not detect a fluorescence signal using confocal laser scanning microscopy (CLSM), although the construct was able to restore SA accumulation after transient expression in *Arabidopsis pbs3* mutant plants (Fig. S8). To investigate the biochemical relationship of *ICS1* and *PBS3* further, we fused the transit peptide of ICS1 (6) to the N-terminus of PBS3 to obtain a chloroPBS3-YFP construct. When ICS1-CFP and chloroPBS3-YFP were transiently co-expressed in Arabidopsis *efr* mutant leaves, they were observed to co-localize in chloroplasts (Fig. 4A). We therefore utilized the fusion protein constructs to monitor the SA formation in *Arabidopsis eds5-3* mutant plants. Strikingly, transient expression of ICS1 together with chloroPBS3 restored SA accumulation. In contrast, the native PBS3 alone or in combination with ICS1 could not restore SA accumulation in *eds5-3* plants (Fig. 4B). This strongly suggests that *EDS5* is responsible for the export of ICS1-derived ISC from the plastidial stroma into the cytosol, where it is further converted by PBS3 (Fig. 4C). This would also explain why SA does not accumulate in *eds5* mutants (Fig. 1A) (*7*). The need for additional ICS1 to restore SA accumulation in combination with chloroPBS3 may be explained by the inhibitory properties of SA towards PBS3 (*11*). As shown in the crystal structure of PBS3 (*16*), SA binds to the same pocket as ISC (Fig. S6). In order to overcome the competitive inhibition, transiently expressed ICS1 is required to produce sufficient amounts of ISC, which subsequently can be transformed by PBS3. Taken together, these data reveal not only how, but also where SA is synthesized at the subcellular level.

By studying SA formation in the autoimmune mutant *snc2-1D npr1-1 pbs3-1*, we were able to identify ISC as the substrate for PBS3 (Fig. 1E). Heterologous expression and purification of PBS3 and ICS1 enabled us to study PBS3 *in vitro*. Thereby we found that PBS3 utilizes ISC as a substrate to conjugate it with glutamate to yield ISC-9-Glu (Fig. 2A). Kinetic analyses (Fig. 2D) as well as *in silico* studies (Fig. S6) confirmed the preference of PBS3 towards ISC as its native substrate. We further observed that the PBS3-derived ISC-9-Glu decays into SA and 2HNG in an enzyme independent manner and ten times faster than its precursor ISC (Fig. 3G). Supporting our *in vitro* findings, we were able to detect ISC-9-Glu as well as 2HNG *in planta* (Fig. 3A and B). Finally, we could show why *ICS1*, *EDS5* and *PBS3* are all required for pathogen induced SA formation (Fig. 4B). While plastidial ICS1 is converting CA into ISC, EDS5 is required to transport ISC from the plastid into the cytosol, where it is conjugated by PBS3 to ISC-9-Glu.

An overwhelming number of studies show the central role of SA for plant immunity. Despite extensive efforts to decipher the biosynthesis of SA, it was not possible so far to reconstitute SA with plant enzymes only. Our study now reveals the functions of EDS5 and PBS3 in the SA biosynthesis and completes the pathogen-induced SA biosynthesis pathway in *Arabidopsis* (Fig. 4C). Additionally, it explains the lack of IPLs in plant genomes. As PBS3 homologues are widespread throughout the plant kingdom (*24*), we uncovered here (Fig. 4C) most likely the general principle of SA biosynthesis in higher plants. In addition, our study also uncovered a novel mode of biosynthesis of a phytohormone. The enzymatically catalyzed formation of SA by pyruvate lyase from either CM or ISC in bacteria was proposed to follow a general base mechanism (*25*). In contrast, the formation of ISC-9-Glu in higher plants brings an intramolecular base directly close enough to the ether oxygen, resulting in a non-enzymatic

heterolytic C-O cleavage. More precisely, the two residues in question are brought in close proximity to each other by two additional hydrogen bonds. These are formed by the two carboxyl groups of the glutamyl moiety which keep the side chain of ISC-9-Glu close to the ring structure. A similar conformation was previously shown to enhance the lyase activity of an bacterial IPL enzyme (*26*), strongly suggesting that ISC-9-Glu automatically forms a transition state that is otherwise found in the active site of bacterial IPLs. This non-enzymatic final step in the production of a key regulatory compound like SA has the advantage that a decay process is uni-directional and that unspecific side reactions, which are typical for IPL enzymes (*27*), are thus highly unlikely (*28*). In bacteria, SA occurs as an intermediate in siderophore biosynthesis (*25*). These iron chelators are essential for the survival and pathogenicity of the microbes. It is tempting to speculate that the reaction mechanism found here occurs in pathogens also and thus may present as a potential new target for antibiotics (*29*).

References:

1. D. M. A. Dempsey, D. F. Klessig, *Trends Plant Sci.* **17**, 538 (2012).
2. I. A. Vos, C. M. J. Pieterse, S. C. M. van Wees, *Plant Pathology* **62**, 43 (2013).
3. S. Z. El-Basyouni, D. Chen, R. Ibrahim, A. Neish, G. Towers, *Phytochemistry* **3**, 485 (1964).
4. H. Klämbt, *Nature* **196**, 491 (1962).
5. M. C. Wildermuth, J. Dewdney, G. Wu, F. M. Ausubel, *Nature* **414**, 562 (2001).
6. C. Garcion *et al.*, *Plant Physiol.* **147**, 1279 (2008).
7. M. Serrano *et al.*, *Plant Physiol.* **162**, 1815 (2013).
8. D. M. A. Dempsey, A. C. Vlot, M. C. Wildermuth, D. F. Klessig, *The Arabidopsis Book*, e0156 (2011).
9. G. Jagadeeswaran *et al.*, *Plant J.* **51**, 234 (2007).
10. P. E. Staswick, I. Tiryaki, M. L. Rowe, *Plant Cell* **14**, 1405 (2002).
11. R. A. Okrent, M. D. Brooks, M. C. Wildermuth, *J. Biol. Chem.* **284**, 9742 (2009).
12. Y. Zhang *et al.*, *Plant Cell* **22**, 3153 (2010).
13. M. Bartsch *et al.*, *J. Biol. Chem.* **285**, 25654 (2010).
14. M. S. DeClue, K. K. Baldridge, P. Kast, D. Hilvert, *J. Am. Chem. Soc.* **128**, 2043 (2006).
15. Q. Chen, C. S. Westfall, L. M. Hicks, S. Wang, J. M. Jez, *J. Biol. Chem.* **285**, 29780 (2010).
16. C. S. Westfall *et al.*, *Science* **336**, 1708 (2012).
17. C. Nawrath, *Plant Cell* **14**, 275 (2002).
18. K. Nobuta *et al.*, *Plant Physiol.* **144**, 1144 (2007).
19. O. Emanuelsson, H. Nielsen, S. Brunak, G. Von Heijne, *J. Mol. Biol.* **300**, 1005 (2000).
20. I. Small, N. Peeters, F. Legeai, C. Lurin, *Proteomics* **4**, 1581 (2004).
21. J. Ludwig-Müller, S. Jülke, N. M. Bierfreund, E. L. Decker, R. Reski, *New Phytol.* **181**, 323 (2009).
22. M. Ostrowski, M. Świdziński, A. Ciarkowska, A. Jakubowska, *Acta Physiol. Plant.* **36**, 3029 (2014).
23. C. Zipfel *et al.*, *Cell* **125**, 749 (2006).
24. R. A. Okrent, M. C. Wildermuth, *Plant Mol. Biol.* **76**, 489 (2011).
25. C. T. Walsh, J. Liu, F. Rusnak, M. Sakaitani, *Chemical Reviews* **90**, 1105 (1990).
26. S. Martí *et al.*, *J. Am. Chem. Soc.* **131**, 16156 (2009).

27. Q. Luo, K. M. Meneely, A. L. Lamb, *J. Am. Chem. Soc.* **133**, 7229 (2011).
28. M. A. Keller, G. Piedrafita, M. Ralser, *Curr. Opin. Biotechnol.* **34**, 153 (2015).
29. A. L. Lamb, *Biochim. Biophys. Acta* **1854**, 1054 (2015).

Acknowledgments: We are grateful to Volker Lipka and Elena Petutschnig (University of Goettingen) for providing infrastructure and support for confocal microscopy (Deutsche Forschungsgemeinschaft (DFG) INST 186/1277-1 FUGG), to Jane Parker (MPIPZ Cologne) for pXCSG-YFP/CFP destination vectors, to Amelie Kelly and Dierk Scheel for critical reading the manuscript, and to Egon Fanghänel for advice on chemical decay. **Funding:** This research has been funded by the DFG (IRTG 2172 "PRoTECT" program of the Göttingen Graduate Center of Neurosciences, Biophysics, and Molecular Biosciences.) to D.R., Y.D., D.L., M.W., Y.Z., and I.F.; I.F. was additionally supported by DFG excellence initiative (ZUK 45/2010). Y.Z. was supported by Natural Sciences and Engineering Research Council of Canada, Canada Foundation for Innovation, and British Columbia Knowledge Development Fund. **Author contributions:** D.R., Y.D., D.L. K.F., Y.Z., and I.F. conceived and designed the experiments. D.R., Y.D. and L.D. performed the experiments. D.R., Y.D., D.L., K.F., Y.Z., and I.F. analyzed the data, D.R., D.L, K.F., M.W., Y.Z., and I.F. wrote the article. **Competing interests:** Authors declare no competing interests. **Data and materials availability:** All data is available in the main text or the supplementary materials. The authors responsible for distribution of materials integral to the findings presented in this article are: Ivo Feussner (ifeussn@uni-goettingen.de) and Yuelin Zhang (yuelin.zhang@ubc.ca).

Supplementary Materials:

Materials and Methods

Figures S1-S8

Tables S1-S2

References (*1-8*)

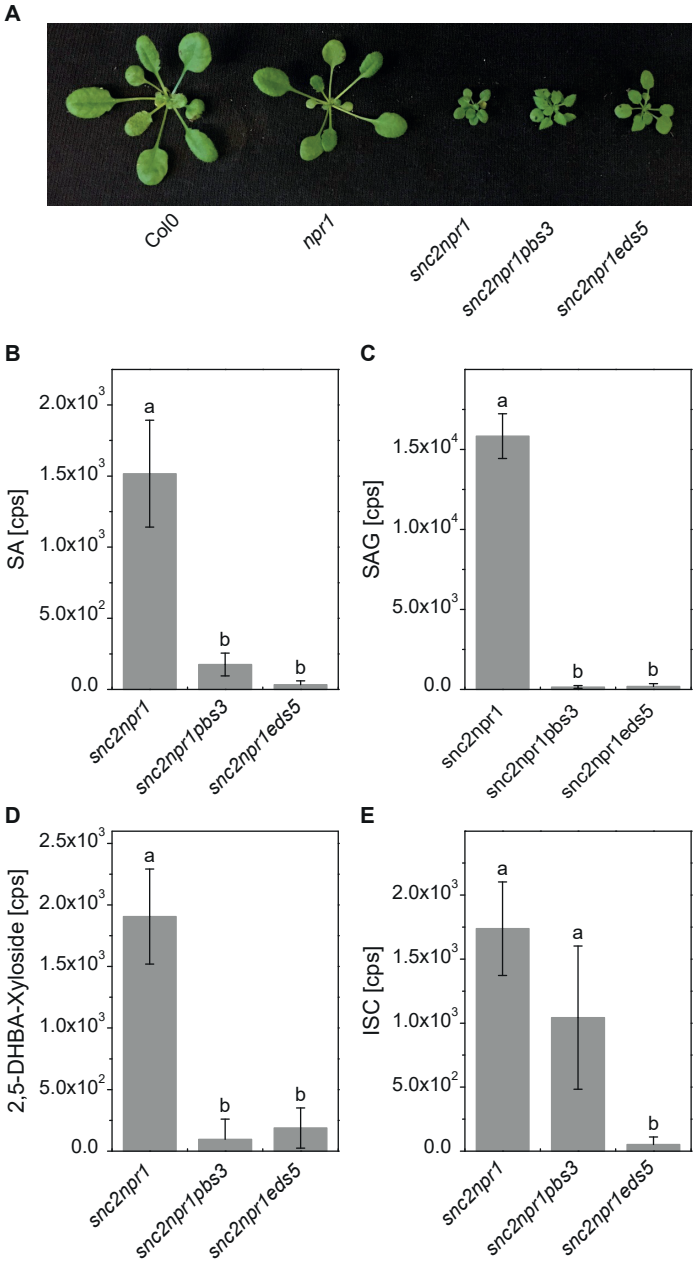

Fig. 1. Analysis of SA-related metabolites in *snc2-1D npr1-1*, *snc2-1D npr1-1 pbs3-1* and *snc2-1D npr1-1 eds5-3*. (**A**) Morphology of four-week-old wild-type (Col-0), *npr1-1*, *snc2-1D npr1-1* (*snc2 npr1*), *snc2-1D npr1-1 pbs3-1* (*snc2 npr1 pbs3*) and *snc2-1D npr1-1 eds5-3* (*snc2 npr1eds5*) plants. (**B-E**) Accumulation of SA (B), SAG (C), 2,5-DHBA-Xyloside (D) and ISC (E) in *snc2 npr1*, *snc2-1 npr1 pbs3* and *snc2 npr eds5*. Relative compound amount (counts per second [cps]) were determined by LC-MS analysis of *Arabidopsis thaliana* leaf samples. Bars represent the mean ± STD of three biological replicates. Statistical differences among replicates are labeled with different letters ($P < 0.05$, one-way ANOVA and post hoc Tukey's Test; $n = 3$).

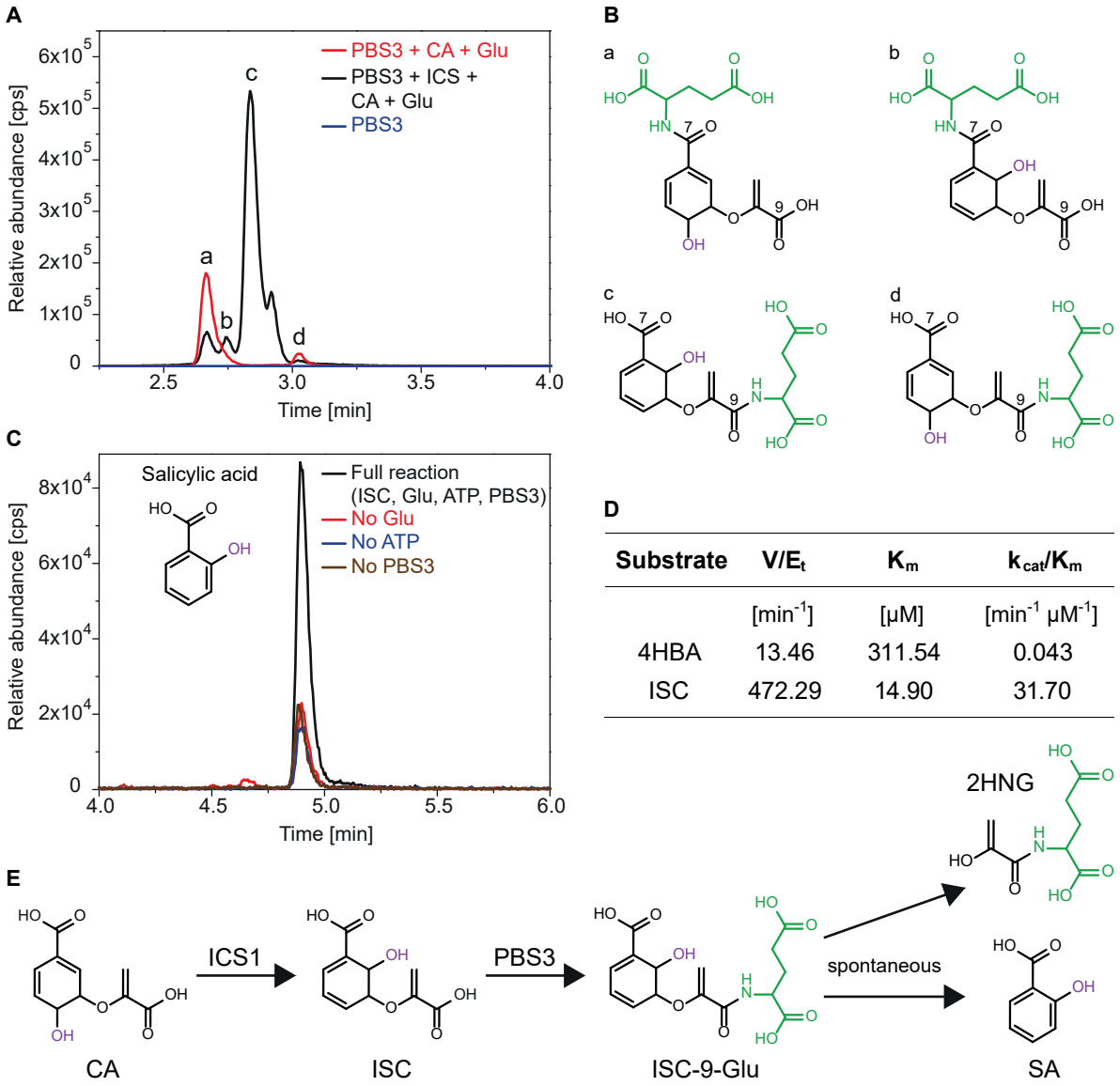

Substrate	V/E_t	K_m	k_{cat}/K_m
	[min^{-1}]	[μM]	[min^{-1} $μM^{-1}$]
4HBA	13.46	311.54	0.043
ISC	472.29	14.90	31.70

Fig. 2. PBS3 catalyzes the production of ISC-9-Glu and SA is formed from the decay of ISC-9-Glu. (**A**) LC-MS analysis of products from activity assays of purified PBS3. The assays were performed with chorismate (CA) and glutamate (Glu) (red line), with CA, Glu and Isochorismate synthase 1 (ICS1, which converts CA to isochorismate (ISC)) (black line) or without acyl substrate (blue line). The extracted ion chromatogram for ISC-9-Glu (*m/z* 354.083) is shown. (**B**) Chemical structures of conjugates formed by PBS3 with Glu (green) and CA (a, d) or ISC (b, c). Depending on the acyl substrate, Glu is preferably conjugated to C7 (for CA) or C9 (for ISC). Structures were solved with MS/MS (Fig. S3). (**C**) Extracted ion chromatogram for SA (*m/z* 137.024) which accumulates in the PBS3 activity assay with ISC, Glu and ATP (black line), but only in minor amount in the absence of Glu (red line), ATP (blue line) or PBS3 (brown line). The presence of SA in the control assays is due to ISC decay in solution. The identity of SA was confirmed by an authentical standard. (**D**) Kinetic parameters of PBS3 with 4HBA or ISC as acyl substrate. Data were obtained spectrophotometrically in triplicates. (**E**) Proposed SA biosynthesis pathway starting from CA. CA is converted by ICS1 to ISC, which is subsequently conjugated to Glu by PBS3. ISC-9-Glu decays spontaneously to SA and 2-hydroxyacryloyl-N-glutamic acid (2HNG).

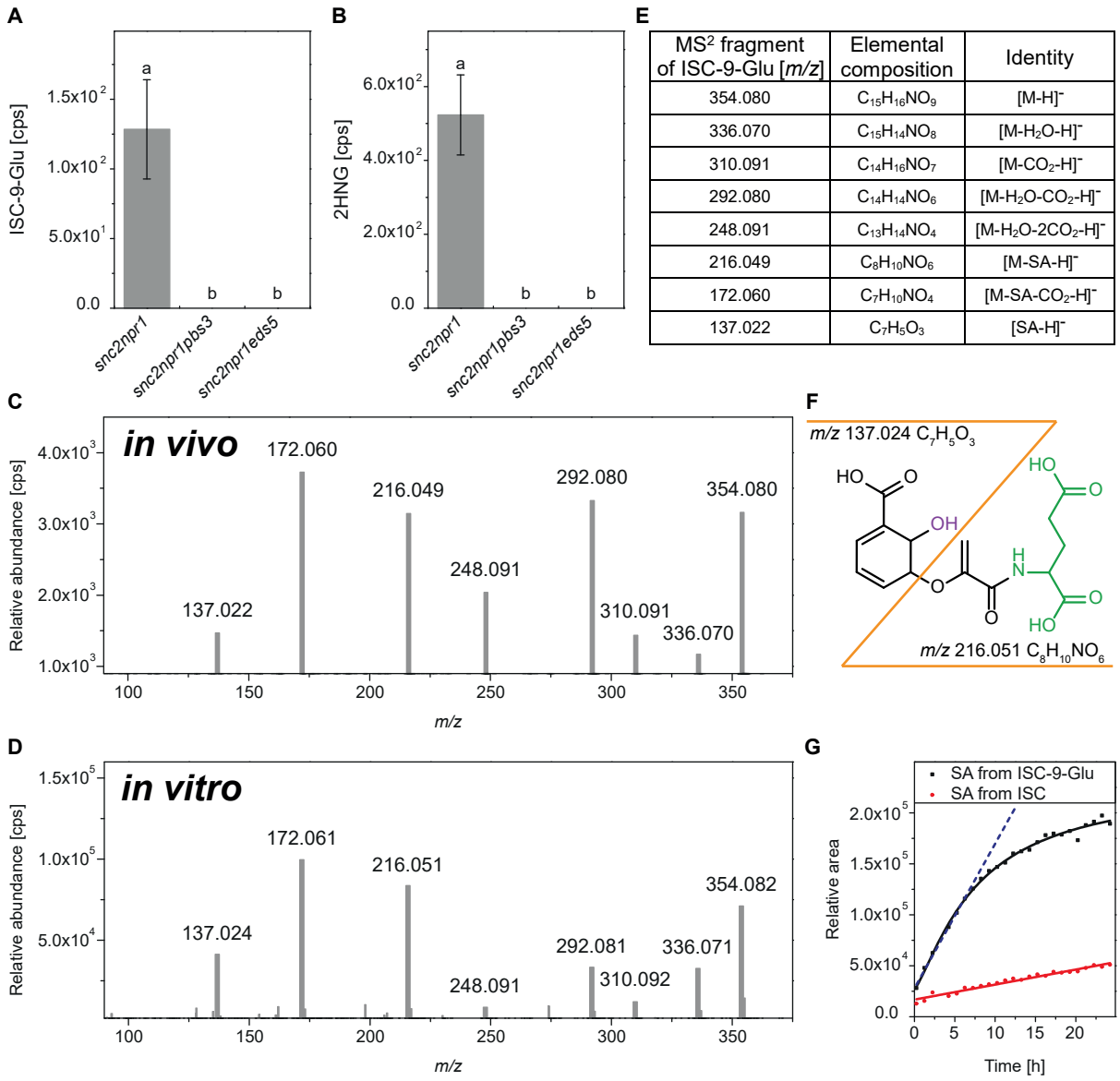

MS² fragment of ISC-9-Glu [*m/z*]	Elemental composition	Identity
354.080	$C_{15}H_{16}NO_9$	$[M-H]^-$
336.070	$C_{15}H_{14}NO_8$	$[M-H_2O-H]^-$
310.091	$C_{14}H_{16}NO_7$	$[M-CO_2-H]^-$
292.080	$C_{14}H_{14}NO_6$	$[M-H_2O-CO_2-H]^-$
248.091	$C_{13}H_{14}NO_4$	$[M-H_2O-2CO_2-H]^-$
216.049	$C_8H_{10}NO_6$	$[M-SA-H]^-$
172.060	$C_7H_{10}NO_4$	$[M-SA-CO_2-H]^-$
137.022	$C_7H_5O_3$	$[SA-H]^-$

Fig. 3. PBS3-dependent production of ISC-9-Glu, 2NHG and SA *in planta*. (**A, B**) Accumulation of ISC-9-Glu (A) and 2-hydroxyacryloyl-N-glutamic acid (2HNG) (B) in *snc2 npr1, snc2 npr1 pbs3* and *snc2 npr1 eds5* plants. Bars represent the mean ± STD of three biological replicates. Statistical differences among replicates are labeled with different letters ($P < 0.05$, one-way ANOVA and post hoc Tukey's Test; n = 3). (**C, D**) MS/MS fragmentation of ISC-9-Glu from *snc2npr1* plant material (C) and PBS3 activity assay (D). (**E**) Annotation list for MS/MS fragments of ISC-9-Glu from *snc2npr1* plant material. Fragments were identified by accurate mass analysis. (**F**) Proposed decay of ISC-9-Glu into SA and 2HNG. (**G**) Time course for the formation of SA from the decay of ISC (red line) and ISC-9-Glu (black line).

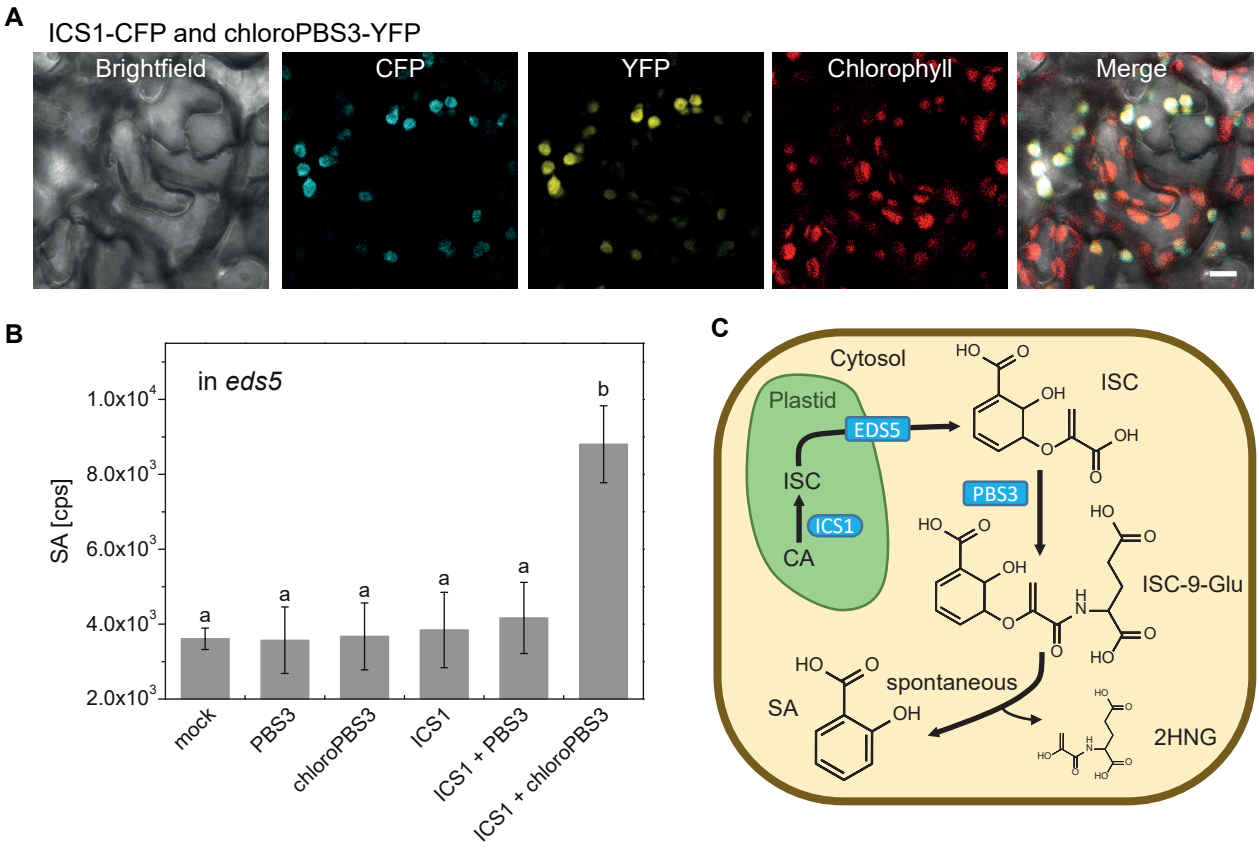

Fig. 4. Plastidial localized PBS3 and ICS1 are sufficient to produce SA in *eds5* plants. (A) Confocal laser scanning microscopy analysis three days after *Agrobacterium*-mediated transient expression of ICS1-CFP and plastidial chloroPBS3-YFP in Arabidopsis *efr* leaves. Scale bar represents 10 µm. **(B)** Transient expression of ICS1 and chloroPBS3 in Arabidopsis *eds5-3* leaves restores the *Agrobacterium tumefaciens* induced SA accumulation. 24 h after infiltration, leaves were collected and metabolites were extracted as described for Metabolite fingerprint analysis. Infiltration medium was used as mock treatment. The SA content was analyzed by UHPLC-Q-TOF-MS. Bars represent the mean ± STD of three biological replicates. Statistical differences among replicates are labeled with different letters ($P < 0.05$, one-way ANOVA and post hoc Tukey's Test; n = 3). (**C**) A working model summarizing pathogen-induced SA biosynthesis in plants.